

SANDIA REPORT

SAND200X-XXXX

Unlimited Release

Printed October 2014

Shock Compression Experiments on Lithium Deuteride Single Crystals

Marcus D. Knudson, Michael P. Desjarlais, Ray W. Lemke

Prepared by
Sandia National Laboratories
Albuquerque, New Mexico 87185 and Livermore, California 94550

Sandia National Laboratories is a multi-program laboratory managed and operated by Sandia Corporation, a wholly owned subsidiary of Lockheed Martin Corporation, for the U.S. Department of Energy's National Nuclear Security Administration under contract DE-AC04-94AL85000.

Approved for public release; further dissemination unlimited.



Sandia National Laboratories

Issued by Sandia National Laboratories, operated for the United States Department of Energy by Sandia Corporation.

NOTICE: This report was prepared as an account of work sponsored by an agency of the United States Government. Neither the United States Government, nor any agency thereof, nor any of their employees, nor any of their contractors, subcontractors, or their employees, make any warranty, express or implied, or assume any legal liability or responsibility for the accuracy, completeness, or usefulness of any information, apparatus, product, or process disclosed, or represent that its use would not infringe privately owned rights. Reference herein to any specific commercial product, process, or service by trade name, trademark, manufacturer, or otherwise, does not necessarily constitute or imply its endorsement, recommendation, or favoring by the United States Government, any agency thereof, or any of their contractors or subcontractors. The views and opinions expressed herein do not necessarily state or reflect those of the United States Government, any agency thereof, or any of their contractors.

Printed in the United States of America. This report has been reproduced directly from the best available copy.

Available to DOE and DOE contractors from
U.S. Department of Energy
Office of Scientific and Technical Information
P.O. Box 62
Oak Ridge, TN 37831

Telephone: (865) 576-8401
Facsimile: (865) 576-5728
E-Mail: reports@adonis.osti.gov
Online ordering: <http://www.osti.gov/bridge>

Available to the public from
U.S. Department of Commerce
National Technical Information Service
5285 Port Royal Rd.
Springfield, VA 22161

Telephone: (800) 553-6847
Facsimile: (703) 605-6900
E-Mail: orders@ntis.fedworld.gov
Online order: <http://www.ntis.gov/help/ordermethods.asp?loc=7-4-0#online>



SAND200X-XXXX
Unlimited Release
Printed October 2014

Shock Compression Experiments on Lithium Deuteride Single Crystals

Marcus D. Knudson, Michael P. Dejsarlais, and Ray W. Lemke
Dynamic Material Properties and HEDP Theory Groups
Sandia National Laboratories
P.O. Box 5800
Albuquerque, New Mexico 87185-MS1195

Abstract

Shock compression experiments in the few hundred GPa (multi-Mabr) regime were performed on Lithium Deuteride (LiD) single crystals. This study utilized the high velocity flyer plate capability of the Sandia Z Machine to perform impact experiments at flyer plate velocities in the range of 17-32 km/s. Measurements included pressure, density, and temperature between ~200-600 GPa along the Principal Hugoniot – the locus of end states achievable through compression by large amplitude shock waves – as well as pressure and density of re-shock states up to ~900 GPa. The experimental measurements are compared with recent density functional theory calculations as well as a new tabular equation of state developed at Los Alamos National Labs.

ACKNOWLEDGMENTS

We would like to thank Dan Dolan for locating the single crystal LiD boule. Michael Siegal (Organization 01114, Nanoscale Sciences Department) is thanked for providing access to the argon glove box used in target preparation. Mark Rodriguez and Jeff Reich (both from Organization 01819, Materials Characterization and Performance) are thanked for performing x-ray diffraction and inductively coupled plasma mass spectrometry measurements, respectively, to characterize the sample material used in these experiments. We also thank the large team at Sandia that contributed to the design and fabrication of the flyer plate loads and the fielding of the shock diagnostics.

CONTENTS

1. Introduction.....	7
2. Experiments	9
2.1. Sample Characterization	9
2.1.1. X-ray Diffraction Measurements.....	9
2.1.2. Inductively Coupled Plasma Mass Spectrometry Measurements	10
2.1.3. Refractive Index	10
2.2. Experimental Configuration.....	11
3. Experimental results.....	15
3.1. Hugoniot Measurements	15
3.1.1. Pressure and Density on the Hugoniot	15
3.1.2. Temperature on the Hugoniot.....	16
3.2. Re-shock Measurements	17
4. Nuclear Driven experiments	19
4.1. Reanalysis	19
4.1.1. Shock Wave Standards	19
4.1.1. Shock Steadiness	20
5. Conclusions.....	21
6. References.....	23
Distribution	25

FIGURES

Figure 1. LiD Theoretical Hugoniots.....	7
Figure 2. XRD pattern from powdered sample.....	9
Figure 3. Lattice parameter as a function of molar mass from Ref. X.	10
Figure 4. Representative velocity profiles from a LiD experiment.	12
Figure 5. Representative SVS data from a LiD experiment.	13
Figure 6. U_s - u_p and P - ρ Hugoniot data for LiD.	16
Figure 7. Temperature vs. P for LiD.....	17
Figure 8. P - ρ re-shock data for LiD.....	18
Figure 9. Reanalysis of nuclear driven experiments.....	20

TABLES

Table 1. LiD Hugoniot data	15
Table 2. LiD re-shock data.....	18

NOMENCLATURE

EOS	Equation of State
LANL	Los Alamos National Labs
LiD	Lithium deuteride
LiH	Lithium hydride
LiOH	Lithium hydroxide
LLNL	Lawrence Livermore National Labs
MHD	Magneto-hydrodynamic
SNL	Sandia National Laboratories
SVS	Streaked visible spectroscopy
VISAR	Velocity interferometer system for any reflector
VPF	Velocity per fringe
XRD	X-ray diffraction

1. INTRODUCTION

Comparison of existing equations of state (EOS) for lithium deuteride (${}^6\text{LiD}$) show a significant discrepancy along the Principal Hugoniot – the locus of end states achievable through compression by large amplitude shock waves – in the several hundred GPa range (several Mbar), as illustrated in Fig. 1. In particular, the often-used EOS models at Lawrence Livermore National Labs (LLNL) and Los Alamos National Labs (LANL), X2040 and S7247, respectively¹, show significant differences even in the few Mbar regime.

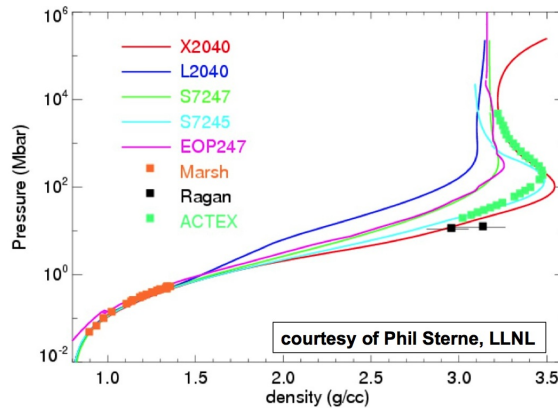


Figure 1. LiD Theoretical Hugoniots.

Several Mbar dynamic pressure in LiD is easily accessible by high-velocity, plate impact experiments at the Sandia Z Machine². Furthermore, the achievable precision and accuracy for Hugoniot measurements in this regime is sufficient to distinguish between the various EOS models. It was therefore determined that a series of shock compression experiments would be performed at the maximum pressure achievable on Z.

These experiments were complicated due to the fact that LiD readily reacts with moisture to form lithium hydroxide (LiOH). This necessitated encapsulation of the samples. We chose to use single crystal α -quartz as a material for encapsulation given that (i) quartz is transparent, allowing optical access to the LiD sample, and (ii) recent Hugoniot³ and adiabatic release measurements in quartz⁴ have enabled the development of quartz as a high-precision standard for use in impedance matching measurements in the multi-Mbar regime. This use of quartz resulted in a negligible increase in uncertainty in the inferred shock response as compared to the precision achievable through direct impact experiments with aluminum flyer plates.

Details of the experiments will be discussed in Section 2, including characterization of the single crystal LiD samples and the experimental configuration. The results of the experiments will be presented in Section 3, including the density, pressure, and temperature along the Hugoniot as well as the density and pressure for re-shock states. A reanalysis of legacy nuclear driven experiments^{5,6} is presented in Section 4 and discussed in the context of the present work. The results are summarized in Section 5.

2. EXPERIMENTS

2.1. Sample Characterization

Single crystal lithium deuteride (LiD) material was obtained from the Crystal Growth Lab at the University of Utah. The crystal was received in boule form and was cleaved within an argon atmosphere to nominally 4 mm in lateral dimensions and ~0.5-0.8 mm in thickness prior to encapsulation within an aluminum and quartz sample holder. Shards from the cleaving process were provided to the Materials Characterization and Performance group (Organization 01819) for further analysis described below.

2.1.1. X-ray Diffraction Measurements

The small LiD shards were ground within a ball mill to prepare a powdered sample. An x-ray diffraction (XRD) pattern was obtained from the powdered sample between 10-100 degrees in two-theta. The resulting XRD pattern is shown in Fig. 2. Diffraction lines were observed from both LiD and LiOH. The outside of the boule had an opaque layer (which was present on some of the shards), presumably a hydroxide layer resulting from reaction of the LiD crystal with either moisture from air prior to the boule being placed in mineral oil for storage, or from moisture within the mineral oil itself. Note that the presence of the hydroxide does not affect the lattice parameter measurement for the LiD crystal, and is thus ignored.

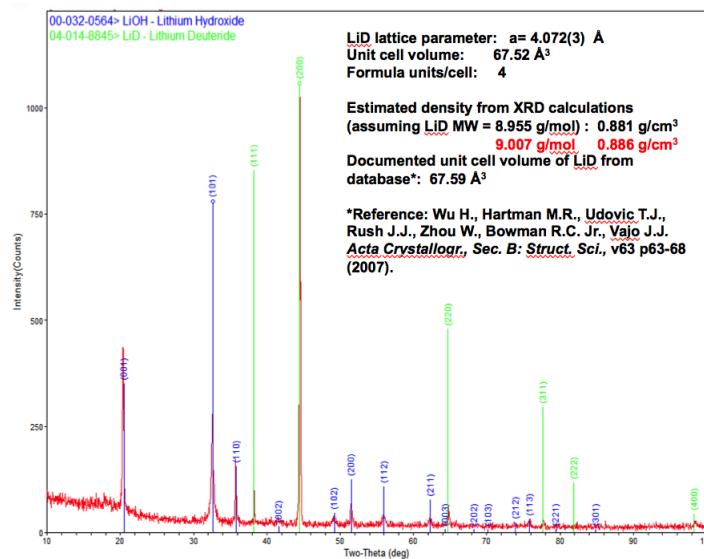


Figure 2. XRD pattern from powdered sample.

The measured lattice was $a = 4.072(3) \text{ \AA}$, resulting in a unit cell volume of $67.52(15) \text{ \AA}^3$. Given that there are 4 LiD pairs per unit cell, the molar volume was determined to be $10.165(22) \text{ cm}^3/\text{mol}$. This allows the density of the sample to be determined given the isotopic fraction of ^6Li to ^7Li in the sample.

2.1.2. Inductively Coupled Plasma Mass Spectrometry Measurements

The small LiD shards were dissolved and used as the sample for inductively coupled plasma mass spectroscopy measurements to determine the isotopic concentration of Li in the actual sample material. The results of the measurement indicated a ${}^6\text{Li}$ composition of between 2.2-2.4% and a ${}^7\text{Li}$ composition of between 97.6-97.8%. This is outside of the normal range from Li, which is a ${}^6\text{Li}$ composition of 7.59(4)% and a ${}^7\text{Li}$ composition of 92.41(4)%, suggesting that the sample is somewhat ${}^7\text{Li}$ rich, but not pure ${}^7\text{Li}$.

It was not possible to determine the isotopic ratio of hydrogen to deuterium. However, the lattice parameter measurement gives some confidence that the sample is in fact highly deuterium enriched. Fig. 3 shows the measured lattice parameters for ${}^6\text{LiH}$, ${}^n\text{LiH}$, ${}^7\text{LiH}$, ${}^6\text{LiD}$, ${}^n\text{LiD}$, and ${}^7\text{LiD}$, as a function of the molar mass⁷ (${}^n\text{Li}$ refers to an isotopic ratio consistent with the natural abundance referred to above). Also shown in Fig. 3 is the measured lattice parameter and the molar mass one would infer for a pure D concentration (red point). Given the significantly larger lattice parameter for pure H concentration (green points) versus the pure D concentration (blue points), clearly the measured lattice parameter for this sample is consistent with the D isotope.

Given this measured Li isotopic concentration, and assumed pure D concentration, and the measured molar volume of the crystal sample, one can determine the density of the sample fairly precisely. The density was determined to be 0.886(2) g/cm³, with an uncertainty of roughly 0.22%.

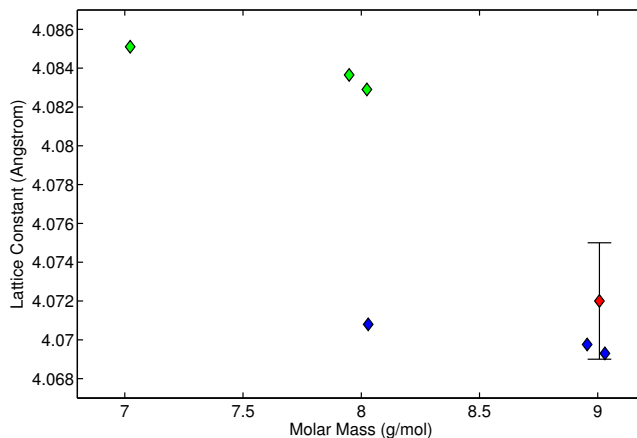


Figure 3. Lattice parameter as a function of molar mass from Ref. X.

2.1.3. Refractive Index

The refractive index is important for proper interpretation of the measured shock velocity in the LiD sample. Given the fact that LiD readily reacts with moisture, an accurate measurement of the refractive index of this particular sample material was not possible. It was determined that the most accurate reported value for the refractive index in the literature was from Ref. 8. That study reported measurement of the refractive index at wavelengths of 435.8, 546.1, and 589.2 nm. Interpolation of these measurements to the wavelength used in this study (532 nm) results in a refractive index of $n = 2.007(5)$. This is the value used in the analysis described below.

2.2. Experimental Configuration

A series of planar, plate-impact shock wave experiments were performed at the Sandia Z Machine², a pulsed power accelerator capable of generating ~ 20 MA currents and ~ 20 MGauss magnetic fields in a short circuit load. The load, which is nominally 4-5 cm in each dimension, is designed to compress the cathode and explode the anode outward as a flyer plate, producing impact velocities in excess of 30 km/s.

Two different load geometries were used in this study. The first, referred to as a coaxial load, has anode plates completely surrounding a central rectangular cathode stalk. Two of these anode plates are designed to be aluminum flyer plates with initial dimensions of approximately 40 mm in height, 20 mm in width, and 1 mm in thickness. The anode box is intentionally aligned asymmetric about the cathode stalk with feed gaps of 1 and 1.4 mm on the two flyer plate sides. This allows for different magnetic pressure in the two gaps, resulting in two different peak flyer plate velocities for each firing of the Z machine, thereby increasing the data return.

The second load geometry, referred to as a stripline load, has a single anode plate opposite a similar cathode plate with a single feed gap. In this case both the anode and cathode are flyer plates with initial dimensions of approximately 36 mm in height, 10 mm in width, and 1 mm in thickness. The benefit of this design is that a significantly larger current density is achieved with respect to the coaxial load, thereby enabling higher flyer plate velocities to be achieved. However, in this case both flyer plates reach essentially the same impact velocity and thus only a single Hugoniot point is obtained for each firing of the Z machine.

Upon discharge of the stored energy within the Marx capacitor banks, a shaped current pulse of ~ 300 ns duration and ~ 20 MA in magnitude is directed through the experimental load. The large current induces a large magnetic field and the resulting $\mathbf{J} \times \mathbf{B}$ force propels the flyer plates outward. Accelerations in the few tenths of a giga-g are produced which drive the panels across a 3-5 mm vacuum gap, reaching impact velocities of ~ 17 -32 km/s depending upon the load geometry and the peak charge voltage. More details regarding the flyer plate launch and the state of the flyer plates at impact can be found in Refs. 9 and 10.

Single crystal LiD samples were cleaved from a boule obtained from the Crystal Growth Lab at the University of Utah. Nominal sample sizes were ~ 4 mm in lateral dimensions and ~ 0.5 -0.8 mm in thickness. Given that LiD readily reacts with moisture to form LiOH, the samples were encapsulated within aluminum and quartz target holders. The holders, the details of which evolved over the experimental series, were essentially aluminum sleeves with single crystal α -quartz windows as end caps. The cleaving and encapsulation were performed within an argon glove box to protect the sample integrity. The target holders were then mounted into a panel back at a prescribed flight distance between 3 and 5 mm, depending upon the desired peak impact velocity.

The flyer plates, α -quartz windows, and LiD samples were diagnosed using a velocity interferometer¹¹ (VISAR – velocity interferometer for any reflector). Since the LiD sample is transparent, the laser light could pass through the target holder and reflect off the flyer plate surface. This allowed an in-line measurement of the flyer velocity from initial motion to impact.

Upon impact a several hundred GPa shock was sent through the α -quartz and LiD sample. This shock was of sufficient magnitude that the resulting plasma became a weak metal, providing significant reflectivity in the visible range. This allowed for direct measurement of the shock velocity of both the α -quartz and LiD with the VISAR diagnostic. Ambiguity in the fringe shift was mitigated through the use of three different VISAR sensitivities or velocity per fringe (VPF) settings. Furthermore, integration of the shock velocity provides a trajectory of the shock through the window and sample, which allows for comparison of the measured thicknesses to those inferred via integration of the shock wave trajectories.

A correction to the sensitivity of the VISAR diagnostic is necessary to obtain the correct shock velocity in both the α -quartz and LiD sample. This is due to the fact that as the shock transits through an initially transparent material the thickness of the un-shocked material through which the laser passes decreases with time, introducing a further Doppler shift in addition to the Doppler shift produced by the moving shock front. It can be shown that for this case the measured apparent velocity must be reduced by a factor equal to the refractive index of the un-shocked material. The refractive index values used in this study for α -quartz¹² and LiD were 1.547 and 2.007, respectively. Representative velocity profiles are shown in Fig. 4.

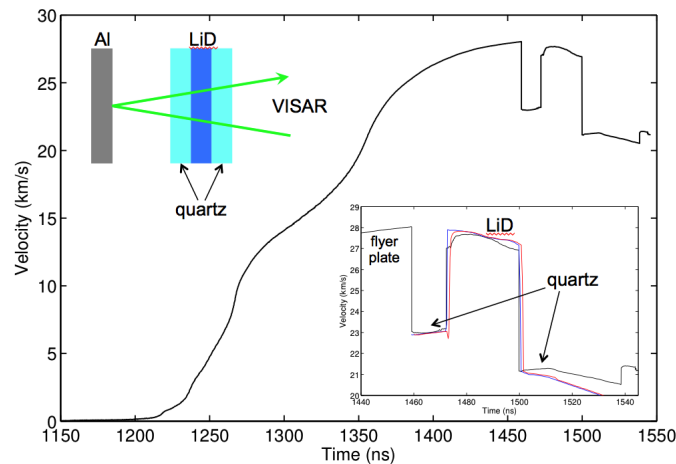


Figure 4. Representative velocity profiles from a LiD experiment.

Note that the shock velocity in the LiD sample has an initial ramp before saturating at a value of ~ 27.5 km/s. This is the result of a small gap between the front quartz window and the LiD sample. Because the LiD readily reacts with moisture it was decided that the quartz/LiD/quartz sample stack would not be glued together with epoxy (the typical procedure). As a result, evidence of small gaps at the front and/or rear interface was observed for all shots. To determine the effect of these gaps on the analysis of the experiments, several simulations of the experiments were performed using the one-dimensional hydro-code CTH. Typical simulations started at the moment of impact with a flyer plate initialized with the density, temperature, and velocity profile obtained from a one-dimensional magneto-hydrodynamic (MHD) optimization of the flyer plate launch similar to that described in Ref. 13. The aluminum flyer plate, the front and rear quartz windows, and the LiD sample were discretized to $0.5 \mu\text{m}$ cell sizes and modeled using SESAME equation of state (EOS) 3700 [14], 7360 [15], and 9004 [16], respectively. Note that SESAME 9004 is a recent EOS for ^7LiD produced by Scott Crockett at LANL.

As can be seen in Fig. 4, the simulations capture qualitatively the behavior observed in the experiment. In particular, the simulated shock velocity in the LiD sample for a simulation that included a 10 μm gap between the front quartz window and the LiD sample (red line) exhibits a similar ramp in velocity prior to saturation, the result of plasma blow off from the shocked quartz front window reverberating between the quartz window and the LiD sample. Comparing this simulation with a second simulation that did not include a gap between the front quartz window and the LiD sample (blue line) suggests that the saturated velocity is a reasonable estimate of the expected shock velocity immediately upon the shock entering the sample.

These small gaps introduced additional complications with the experiment. In particular, the gaps resulted in significant interface reflections, which were especially severe in the first experiment. Given the large refractive index of LiD ($n = 2.007$) dielectric coatings were put on the quartz windows to minimize reflections for the quartz up against $n = 2$. However, with a gap present there are then two interfaces each with two surfaces that go from $n = 2$ to $n = 1$ (quartz/gap and gap/LiD), resulting in a total reflection of $\sim 45\%$ (each surface has a reflection of $\sim 11.1\%$). In an attempt to mitigate these reflections the subsequent target holders were designed such that a mineral oil based index fluid ($n = 1.7$) could be placed between the quartz and LiD sample. In theory this would reduce the overall reflection at the interfaces to $\sim 1\text{-}2\%$.

Emission from the shocked quartz windows and LiD sample were collected in an optical fiber and delivered to a streaked visible spectroscopy (SVS) diagnostic which consisted of a spectrometer coupled to a streak camera to provide spectrally and temporally resolved data. A typical SVS image is shown in Fig. 5. In this image time is running down and wavelength increases to the right. The first bright horizontal band (around 20 mm in the time direction) is emission from the shocked front quartz window. The lighter band (between 20-22 mm) is emission from the shocked LiD sample. The next brighter band (between 22-26 mm) is emission from the shocked rear quartz window. The bright vertical band (at 18 mm in the wavelength direction) corresponds to the 532 nm VISAR laser. The other vertical bands correspond to wavelength and time fiducials. The analysis of these data to infer temperature of the shocked LiD sample will be described in the next section.

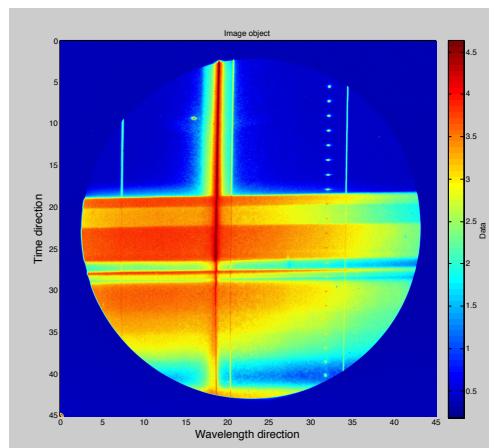


Figure 5. Representative SVS data from a LiD experiment.

3. EXPERIMENTAL RESULTS

3.1. Hugoniot Measurements

3.1.1. Pressure and Density on the Hugoniot

The shocked state of the LiD was determined using the impedance matching technique and the Rankine-Hugoniot jump relations¹⁷, a set of conditions derived by considering conservation of mass, momentum, and energy across a steady propagating shock wave, relating the initial energy E , volume V , and pressure P , with steady-state, post-shock values

$$(E_1 - E_0) = (P_1 + P_0)(V_0 - V_1)/2 \quad (1)$$

$$(P_1 - P_0) = \rho_0 U_s (u_{p1} - u_{p0}) \quad (2)$$

$$\rho_1 = \rho_0 \left[U_s / (U_s - (u_{p1} - u_{p0})) \right] \quad (3)$$

Here ρ , U_s , and u_p denote the density, shock velocity, and particle velocity, respectively, and the subscripts 0 and 1 denote the initial and final values. The shocked state of the quartz drive plate was determined from the known Hugoniot of quartz³ and the measured quartz shock velocity; this defined a point in the P - u_p plane. When the shock transits into the LiD, a release wave propagates back toward the flyer-plate, and thus the state of the drive plate is constrained to lie on a release adiabat of quartz⁴ from this point in the P - u_p plane. Given Eq. (2), the shocked state of the LiD is constrained to lie along a chord in the P - u_p plane with slope given by the product of the measured shock velocity of the LiD, U_{sLiD} , and the known initial density. The intersection of these two curves provides P and u_p ; Eq. (3) then provides ρ in the shocked state. Uncertainties in all kinematic values were determined through a Monte Carlo technique, which utilizes a statistical process for propagation of all random measurement errors and systematic errors in the aluminum and quartz standard. Using this technique, the one-sigma uncertainties in P and ρ for the Hugoniot states were found to be $\sim 0.5\%$ and $\sim 1\%$, respectively.

A total of four plate impact experiments, one coaxial and three stripline, were performed on single crystal LiD. The pertinent parameters for these Hugoniot experiments are listed in Table 1. u_v denotes the measured flyer velocity, and U_{sq1} and U_{sLiD} denote the measured shock velocities in the front quartz window and the LiD sample, respectively. u_p denotes the inferred particle velocity in the LiD, and ρ and P denote the inferred density and pressure of the LiD in the shocked state, respectively.

Table 1. LiD Hugoniot data

Z shot	U_{sq1} (km/s)	U_{sLiD} (km/s)	u_p (km/s)	ρ (g/cm ³)	P (GPa)
Z2586	15.77±0.03	18.92±0.06	11.22±0.07	2.178±0.023	188.1±1.2
Z2497	23.21±0.03	27.63±0.06	18.65±0.08	2.726±0.029	456.5±2.1
Z2497	24.75±0.03	29.55±0.06	20.24±0.09	2.815±0.031	530.0±2.5
Z2577	25.21±0.03	30.29±0.06	20.70±0.09	2.797±0.030	555.6±2.6
Z2692	25.46±0.03	30.54±0.06	20.97±0.09	2.827±0.031	567.5±2.7

The Hugoniot data for LiD are shown in both U_s-u_p and $P-\rho$ in Fig. 6. Also shown are the predicted response from S7247, X2040, SESAME 9004, and recent quantum molecular dynamics (QMD) calculations from Desjarlais.¹⁸ Note that we only had access to the ${}^6\text{LiD}$ EOS models for both S7247 and X2040. To account for the higher molar mass of our samples, which are very close to ${}^7\text{LiD}$, we performed a simple shift in the U_s-u_p response from these models downward by 0.37 km/s. This shift was determined by comparison of QMD calculations for ${}^6\text{LiD}$ and ${}^7\text{LiD}$ as well as comparing SESAME 9001 and 9004, the most recent EOS models for ${}^6\text{LiD}$ and ${}^7\text{LiD}$, respectively, developed at LANL.

These data would suggest that the X2040 EOS is systematically too compressible and the S7247 EOS is significantly too stiff. In contrast, the experimental data are in quite good agreement with the QMD calculations and the SESAME 9004 EOS. One might argue that the data tend to be slightly systematically softer at the highest pressures, however, it is not clear whether such a conclusion is warranted given the statistical significance of such a trend.

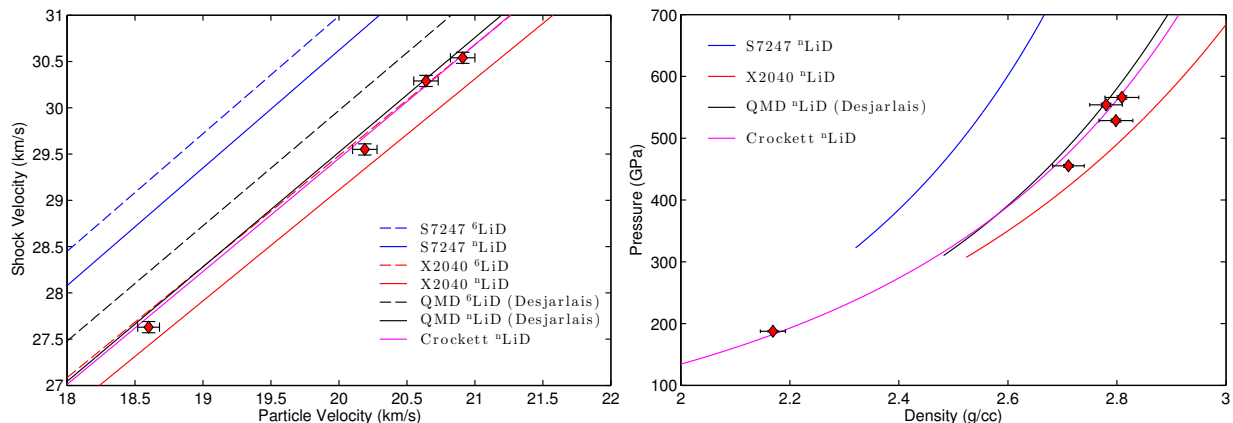


Figure 6. U_s-u_p and $P-\rho$ Hugoniot data for LiD.

3.1.2. Temperature on the Hugoniot

Temperature of the shocked LiD sample was determined by using the emission from the quartz front and rear windows as a temperature standard. Previous shock wave experiments on quartz in the multi-Mbar regime have determined the temperature of quartz as a function of shock speed,¹⁹ enabling quartz to be used as a standard for temperature measurements. Emission from the rear quartz window was used as a calibration for the SVS image. Given the shock velocity in the rear quartz window, the temperature of quartz as a function of shock speed, and the emissivity of quartz in the multi-Mbar regime,¹⁸ a calibration factor can be determined for the SVS image. Furthermore, given the shock velocity in the front quartz window, the temperature of quartz as a function of shock speed, and the emissivity of quartz in the multi-Mbar regime, the emission one would expect to observe from the front quartz window can also be determined. Typically, the expected emission from the front quartz window is greater than what is actually observed; the difference can be attributed to reflections at the two quartz/LiD interfaces (see discussion above). Under the assumption that these two interfaces contribute equally to the reflection losses, we can adjust the observed LiD emission accordingly. Finally, given the emissivity of LiD in the multi-Mbar regime¹⁸ the temperature of the shocked LiD can be determined.

This procedure was followed at each wavelength across the recorded SVS spectrum. The results of four experiments are shown in Fig. 7. The relatively flat inferred temperature across the 450-650 nm spectrum lends confidence in the method used to infer the temperature of the shocked LiD. Note that the large spike near 532 nm is the result of both the VISAR laser and the notch filter used to block the majority of the VISAR laser from the SVS diagnostic. Also shown in Fig. 7 are the inferred temperature as a function of pressure along with three QMD calculations (green diamonds) and the prediction from SESAME 9004 (blue line).

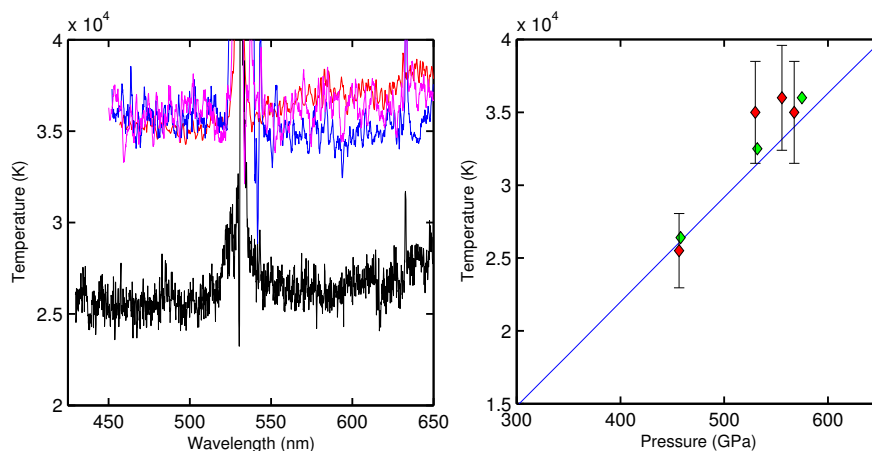


Figure 7. Temperature vs. P for LiD.

3.2. Re-shock Measurements

The compressibility of LiD was further explored by performing re-shock experiments. In four of the Hugoniot experiments described above, the reflected shock from the rear quartz window drove the LiD from a Hugoniot state to a re-shocked state at higher P and ρ . The measured shock velocity in the LiD immediately prior to reflection from the rear quartz window defined the initial shocked state of the LiD. Note that a fit to the Principal Hugoniot data (listed in Table 1) was used to determine the Hugoniot response of LiD; this fit and the measured shock velocity in the LiD sample immediately prior to the shock reflecting from the rear quartz window determined the initial shock state P_1 and u_{p1} . The measured shock velocity in the rear quartz window and the known Hugoniot of quartz provided the double-shocked P and u_p for LiD. The velocity of the second shock in the LiD, U_{sLiD2} , was then determined by evaluating Eq. (2) using the change in pressure and particle velocity, $(P_2 - P_1)$ and $(u_{p2} - u_{p1})$. Given the second shock velocity in the LiD, the first shock ρ , and $(u_{p2} - u_{p1})$, the re-shock density was determined from Eq. (3). Using the Monte Carlo technique, the one-sigma uncertainties in P and ρ for the re-shock states were found to be $\sim 0.5\%$ and $\sim 1.5\%$, respectively. Although the uncertainty for the re-shock data is larger than that for the principal Hugoniot data (entirely due to the larger uncertainty in the initial state), the accuracy of the present data will provide a stringent constraint of the re-shock response of LiD in the multi-Mbar regime.

The pertinent parameters for these re-shock experiments are listed in Table 2. U_{sLiD} and U_{q2} denote the measured shock velocities in the LiD sample and the rear quartz window,

respectively. ρ_1 and P_1 denote the density and pressure of the LiD in the Hugoniot state immediately prior to the shock reflecting from the rear quartz window, respectively, and ρ_2 and P_2 denote the inferred density and pressure of the LiD in the re-shocked state, respectively.

Table 2. LiD re-shock data.

Z shot	U_{sLiD} (km/s)	U_{sq2} (km/s)	ρ_1 (g/cm ³)	P_1 (GPa)	ρ_2 (g/cm ³)	P_2 (GPa)
Z2497	26.94±0.06	21.33±0.03	2.664±0.023	429.1±2.6	3.464±0.056	728.4±3.9
Z2497	28.60±0.06	22.66±0.03	2.744±0.024	491.0±2.8	3.589±0.057	837.1±4.3
Z2692	29.65±0.06	23.43±0.03	2.797±0.025	532.0±3.0	3.696±0.060	904.0±4.5
Z2577	29.85±0.06	23.56±0.03	2.806±0.025	540.0±3.0	3.730±0.061	915.6±4.6

The re-shock data for LiD are shown in Fig. 8, where first and second shock states are shown in blue. The red points correspond to the principal Hugoniot measurements listed in Table 1 and plotted in Fig. 6. Also shown are the Principal Hugoniot from Desjarlais (black line) and SESAME 9004 (magenta line) and three calculated re-shock states from Desjarlais (black points) and two re-shock Hugoniot from SESAME 9004 (magenta lines). Note that the re-shock results appear to be systematically softer than the QMD predictions, in accordance with the trend observed in the Principal Hugoniot data. Since we did not have access to a ⁷LiD version of either S7247 or X2040 we were unable to make re-shock comparisons with these models.

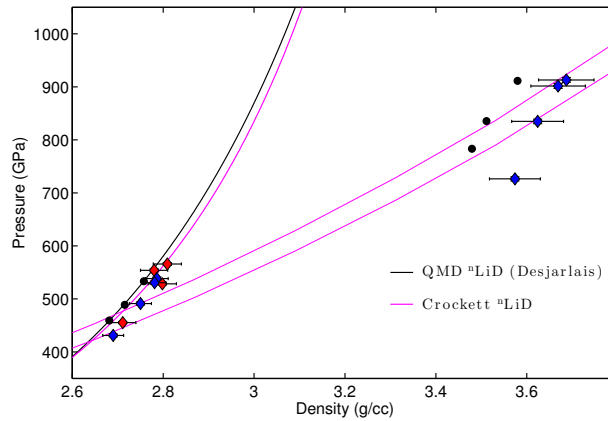


Figure 8. P- ρ re-shock data for LiD.

4. NUCLEAR DRIVEN EXPERIMENTS

4.1. Reanalysis

Ragan published results of nuclear driven experiments on both ${}^6\text{LiD}$ [5] and ${}^6\text{LiH}$ [6]. Both of these publications suggest a somewhat more compressible response than the present work as well as the QMD Hugoniot for ${}^6\text{LiD}$ and ${}^6\text{LiH}$ and the SESAME 9001 Hugoniot for ${}^6\text{LiD}$ [16]. However, two aspects of the experiments and analysis bring into question the reported results; (i) the treatment of the shock standards upon release, and (ii) the steadiness of the shock and how that was accounted for in the analysis. Both of these aspects of the experiments tend to result in a softer response, and thus a reanalysis tends to result in a stiffer response, bringing the inferred results into better agreement with the recent calculations and experiments.

4.1.1. Shock Wave Standards

Both molybdenum and beryllium were used as standards for the ${}^6\text{LiD}$ experiments reported in Ref. 5. According to the paper Sesame tables 2981 and 2020 were used for molybdenum and beryllium, respectively. Table 2981 was a new table developed by Kerley specifically for the analysis of this particular nuclear-driven experiment. Comparing the Hugoniot response of 2981 and the older 2980 to experimental data in the several TPa range from Ragan,²⁰ Al'tshuler,²¹ Trunin,²² and Mitchell²³ (the Mitchell results were reanalyzed²⁴ with a more reasonable aluminum Hugoniot, resulting in slightly higher inferred pressure and density) shows that 2981 is significantly stiffer than 2980 and is in better agreement with available data.

However, as Ragan points out in the paper, the release isentropes for 2981 and 2980 from the inferred shocked states of the molybdenum base plate (which differ in particle velocity by 3% for the two tables) are nearly identical in the vicinity of the ${}^6\text{LiD}$ Hugoniot. This is rather surprising. One would expect the release from these pressures and temperatures (5 TPa and 15 eV) to be adequately described by a Mie-Gruneisen (MG) model with Gamma of $\sim 2/3$. Comparing the releases from 2981 and 2980 with such a model suggests that 2981 is the problem, inferring a release path that exhibits too high a particle velocity for a given pressure. To perform the reanalysis of this datum the 2981 Hugoniot was used as a reference for a MG model with Gamma of $2/3$.

For the beryllium standard experiment Ragan used table 2020. I evaluated several different beryllium tables with respect to Hugoniot data in the few TPa range from Ragan⁵ and Nellis²⁵ (again the Nellis data was reanalyzed²⁴ with a more reasonable aluminum Hugoniot, resulting in slightly higher inferred pressure and density). The most reasonable agreement with these data was found for table 2010 [26], which is a table developed by Kerley circa 2002. To perform a reanalysis of this datum 2010 Hugoniot was used as a reference for a MG model with Gamma of $2/3$. The final experiment⁶, used carbon as the standard. Unfortunately, there is no Hugoniot data in the TPa range for comparison, and so table 7831 was used, the same table used by Ragan in the analysis. However, again the 7831 Hugoniot was used as the reference for a MG model with Gamma of $2/3$.

4.1.1. Shock Steadiness

Ragan noted that there was evidence of attenuation of the shock waves as they traversed the various layers (Mo/LiD/Be and Mo/Be/LiD for the ${}^6\text{LiD}$ experiments⁵). To account for this, it appears that Ragan assumed a 1% drop in shock velocity across the various samples. He then used the appropriate upshifted or downshifted velocity as the shock velocity at the front or rear of the material when performing the impedance match calculation. This correction results in a stiffer response than one would get if they were to use the average shock velocity obtained directly from the transit time measurement, ignoring the effects of attenuation. Furthermore, if one were to assume a larger attenuation (i.e. a larger percentage drop in shock velocity across the sample), the corrected result would be even stiffer.

It is interesting that the assumed attenuation for the ${}^6\text{LiH}$ experiment,⁶ 3%, is significantly larger than that assumed for the ${}^6\text{LiD}$ experiments.⁵ This seems strange given that “the experimental configuration for the EOS package was nearly identical to that used in (the ${}^6\text{LiD}$ study).” Indeed the thicknesses of the lead, molybdenum, and the various samples were essentially the same for the two studies. The only difference being that the shocked state in the molybdenum was higher (~6 TPa) for the ${}^6\text{LiH}$ experiment than it was (~5 TPa) for the ${}^6\text{LiD}$ experiments. It is not clear why the attenuation was assumed to be larger, but it does question the magnitude of the attenuation used to correct the ${}^6\text{LiD}$ data. If one were to assume that the magnitude of the attenuation was underestimated in the ${}^6\text{LiD}$ experiments, the correction for attenuation would be larger and would bring the inferred results closer in line with the recent QMD calculations for ${}^6\text{LiD}$, as shown in Fig. 9. This figure shows the reanalyzed results assuming various levels of attenuation along with the QMD Hugoniot for ${}^6\text{LiH}$, ${}^6\text{LiD}$, and ${}^7\text{LiD}$. Given this exercise, it can be concluded that the results from the nuclear driven experiments are not inconsistent with the recent theoretical and experimental studies of LiD.

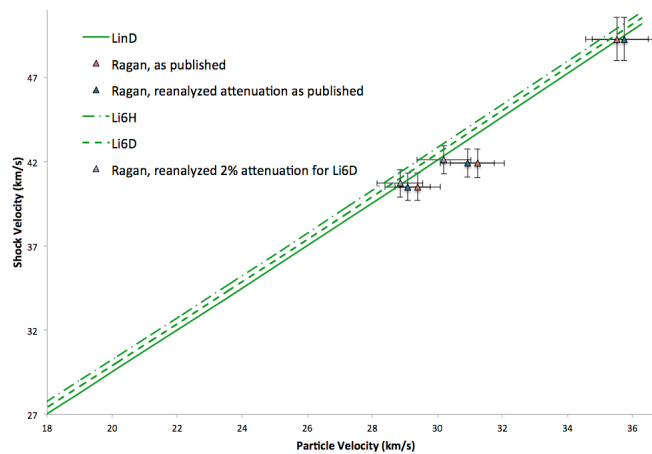


Figure 9. Reanalysis of nuclear driven experiments.

5. CONCLUSIONS

A series of shock compression experiments were performed on LiD single crystals using the high velocity flyer plate capability of the Sandia Z Machine. Pressure, density, and temperature were measured along the Principal Hugoniot between ~200-600 GPa. Pressure and density of re-shock states were also measured up to ~900 GPa. These data were found to be in disagreement with the often-used equation of state (EOS) models at LLNL and LANL, X2040 and S7247, respectively. In contrast, the results were found to be in reasonably good agreement with recent quantum molecular dynamics calculations performed at SNL as well as a new EOS model, SESAME 9004, developed at LANL. Finally, legacy nuclear driven experiment on ${}^6\text{LiD}$ and ${}^6\text{LiH}$ were reanalyzed, using modern EOS tables and better release models. The reanalyzed data were found to be consistent with the recent theoretical and experimental work on LiD.

6. REFERENCES

1. Phil Sterne, private communication.
2. M. K. Matzen, et al. Pulsed-Power-Driven High Energy Density Physics and Inertial Confinement Fusion Research, in *Phys. Plasmas*, vol. 12, pp. 055503, 2005.
3. M. D. Knudson and M. P. Desjarlais, Shock Compression of Quartz to 1.6 TPa: Redefining a Pressure Standard, in *Phys. Rev. Lett.*, vol. 103, pp. 225501, 2009.
4. M. D. Knudson and M. P. Desjarlais, Adiabatic Release Measurements in α -quartz Between 300 and 1200 GPa: Characterization of α -quartz as a Shock Standard in the Multimegabar Regime, in *Phys. Rev. B*, vol. 88, pp. 184107, 2013.
5. C. E. Ragan III, Shock Compression Measurements at 1 to 7 TPa, in *Phys. Rev. A*, vol. 25, pp. 3360-3375, 1982.
6. C. E. Ragan III, Shock-Wave Experiments at Threefold Compression, in *Phys. Rev. A*, vol. 29, pp. 1391-1402, 1984.
7. XRD
8. Eugene Staritzky and D. I. Walker, Crystallographic Data. 124. Lithium Hydride, LiH; 125. Lithium Deuteride, LiD, in *Anal. Chem.*, vol. 28, pp. 1055-1055, 1956.
9. R. W. Lemke, M. D. Knudson, C. A. Hall, T. A. Haill, M. P. Desjarlais, J. R. Asay, and T. A. Mehlhorn, Characterization of Magnetically Accelerated Flyer Plates, in *Phys. Plasmas*, vol. 10, pp. 1092-1099, 2003.
10. R. W. Lemke, M. D. Knudson, A. C. Robinson, T. A. Haill, K. W. Struve, J. R. Asay, and T. A. Mehlhorn, Self-Consistent, Two-Dimensional, Magnetohydrodynamic Simulations of Magnetically Driven Flyer Plates, in *Phys. Plasmas*, vol. 10, pp. 1867-1874, 2003.
11. L. M. Barker and R. E. Hollenbach, Laser Interferometer for Measuring High Velocities of Any Reflecting Surface, in *J. Appl. Phys.*, vol. 43, pp. 4669-4675, 1972.
12. G. Ghosh, Dispersion-Equation Coefficients for the Refractive Index and Birefringence of Calcite and Quartz Crystals, in *Optics Comm.*, vol. 163, pp. 95-102, 1999.
13. R. W. Lemke, M. D. Knudson, D. E. Bliss, K. Cochran, J.-P. Davis, A. A. Giunta, H. C. Harjes, and S. A. Slutz, Magnetically Accelerated, Ultrahigh Velocity Flyer Plates for Shock Wave Experiments, in *J. Appl. Phys.*, vol. 98, pp. 073530, 2005.
14. G. I. Kerley, Theoretical Equation of State for Aluminum, in *Int. J. Impact Eng.*, vol. 5, pp. 441, 1987.
15. G. I. Kerley, *Equation of State for Composite Materials*, Kerley Publishing Services Report No. KPS99-4, 1999.
16. Scott Crockett, private communication.
17. G. E. Duvall and R. A. Graham, Phase Transitions Under Shock-Wave Loading, in *Rev. Mod. Phys.*, vol. 49, pp. 523, 1977.
18. M. P. Desjarlais, private communication.
19. P. M. Celliers, P. Loubeyre, J. H. Eggert, S. Brygoo, R. S. McWilliams, D. G. Hicks, T. R. Boehly, R. Jeanloz, and G. W. Collins, Insulator-to-Conducting Transition in Dense Fluid Helium, in *Phys. Rev. Lett.*, vol. 104, pp. 184503, 2010.
20. C. E. Ragan, M. G. Silbert, and B. C. Diven, Shock Compression of Molybdenum to 2.0 TPa by Means of a Nuclear Explosion, in *J. Appl. Phys.*, vol. 48, pp. 2860-2870, 1977.
21. L. V. Al'tshuler, A. A. Bakanova, I. P. Dudoladov, E. A. Dynin, R. F. Trunin, and B. S. Chekin, Shock Adiabats for Metals. New Data, Statistical Analysis and General

- Regularities, in *Zh. Prikl. Mekh. Tekhn. Fiz.*, vol. 2, pp. 3-34, 1981 [in Russian] (*J. Appl. Mech. Tech. Phys.*, vol. 22, pp. 145, 1981).
22. R. F. Trunin, G. V. Simakov, Yu. N. Sutulov, A. B. Medvedev, B. D. Rogozkin, and Yu. E. Fedorov, Compression of Porous Metals in Shock Waves, in *Zh. Eksp. Teor. Fiz.*, vol. 96, pp. 1024-1038, 1989 [in Russian] (*Sov. Phys. – JETP*, vol. 69, pp. 580-588, 1989).
 23. A. C. Mitchell, W. J. Nellis, J. A. Moriarty, R. A. Heinle, N. C. Holmes, R. E. Tipton, and G. W. Repp, Equation of State of Al, Cu, Mo, and Pb at Shock Pressures up to 2.4 TPa (24 Mbar), in *J. Appl. Phys.*, vol. 69, pp. 2981-2986, 1991.
 24. M. D. Knudson, private communication.
 25. W. J. Nellis, J. A. Moriarty, A. C. Mitchell, and N. C. Holmes, Equation of State of Beryllium at Shock Pressure of 0.4-1.1 TPa (4-11 Mbar), in *J. Appl. Phys.*, vol. 82, pp. 2225-2227, 1997.
 26. G. I. Kerley, *Equation of State for Be, Ni, W, and Au*, Sandia Report, Report No. SAND2003-3784, 2003.

DISTRIBUTION

4 Lawrence Livermore National Laboratory
Attn: N. Dunipace (1)
P.O. Box 808, MS L-795
Livermore, CA 94551-0808

1	MS1189	John Benage	01646
1	MS1195	Marcus Knudson	01646
1	MS0899	Technical Library	9536 (electronic copy)
1	MS0359	D. Chavez, LDRD Office	1911

